Electrospun Nanofibrils Surface-Decorated with Photo-Cross-Linked Hyaluronic Acid for Cell-Directed Assembly

Wanho Cho, Yeonju Park, Young Mee Jung, Ju Hyun Park, Jongmin Park, and Hyuk Sang Yoo*

ACCESS | Metrics & More | Article Recommendations | SI Supporting Information

ABSTRACT: Hyaluronic acid (HA) was chemically immobilized on the surface of electrospun nanofibrils to form a cell/NF complex. Poly(caprolactone) (PCL) was electrospun into nanofibrous mats that were subsequently aminolyzed into nanofibrils. The aminolyzed nanofibrils were surface-decorated with methacrylated HA via Michael type addtion and by photo-cross-linking. Fourier transform infrared spectroscopy revealed the presence of HA on the surface of the nanofibrils. The thermogravimetric and colorimetric analyses indicate that the degree of HA immobilization could be varied by varying the photo-cross-linking duration. Thus, on increasing the photo-cross-linking duration, the swelling ratios increased gradually, and the surface charge of the decorated nanofibrils decreased. NIH3T3 cells and surface-decorated nanofibrils spontaneously assembled into the cell/NF complex. A higher degree of surface-immobilized HA enhanced cell viability and proliferation compared to nanofibrils without surface-immobilized HA. Thus, we envision that HA-immobilized nanofibrils can be employed as a tissue-engineering matrix to control cell proliferation and differentiation.
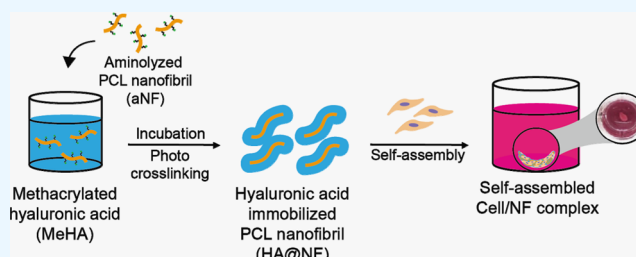
INTRODUCTION

Electrospinning is a potential strategy for fabricating nonwoven fibrous matrices conveniently and economically.[1−3] Various synthetic and natural polymers have been used to electrospin fibrous matrices.[4−6] However, several natural polysaccharides, such as hyaluronic acid (HA) and chitosan, are highly viscous; therefore, electrospinning such polymers to form continuous fibers is challenging.[7−9] To overcome these difficulties, natural polymers are often dissolved in strong acid or base solutions to weaken the electrostatic interactions between the molecules, which reduces the viscosity of the solution and allows better electrospinning.[8,10] Thus, solvents such as trifluoroacetic acid (TFA) and trifluoroethanol (TFE) are used to electrospin natural polymers.[11,12] However, biomedical devices composed of nanofibers that were electrospun with those solvents can cause severe toxicity in the blood, reproductive system, bladder, brain, upper respiratory tract, and eyes if a minor amount of the solvent is present in the nanofibers. Another approach to circumvent this problem is to blend synthetic polymers that exhibit good electrospinnability with natural polymers. Thus, poly(vinyl alcohol) (PVA) and poly(ethylene oxide) (PEO) have been extensively employed as additive polymers to fabricate a natural polymer containing electrospun nanofibers.[13−15] Nanofibers with different volume ratios of chitosan to PVA were fabricated. All blend solutions except the pure chitosan solution were electrospinnable, and nanofibers made from these solutions showed bead-free and uniform morphology. However, the blend solution having a high chitosan to PVA ratio showed low throughput for electro-

spinning because of its high viscosity.[16] PEO was also employed as a modifier to reduce the unusually high viscosity of HA, and it facilitated the fabrication of nanofibrous HA derivative scaffolds. Nanofibers with an HA to PEO ratio of 4:1 resulted in an uneven fiber formation and high bead density; however, when the ratio was reduced to 1:1, the bead density was significantly reduced, and uniform fibers were obtained.[17] The amount of natural polymers in the blend solution should be reduced when the amount of synthetic polymers is increased for better electrospinning, which can substantially decrease the effect of the biological activity of natural polymers on the electrospun nanofibers.

Electrospun nanofibers exhibit surface hydrophobicity and lack active sites that can be further immobilized with biomolecules. To overcome these difficulties, we previously reported the hydrolysis and surface decoration of nanofibers so that the fragmented nanofibers can easily interact with the cells for the three-dimensional (3D) assembly of tissue constructs.[18] After optimizing the conditions for aminolysis of PCL nanofibers, in addition to the increased hydrophilicity, considerable levels of primary amines can be grafted on the
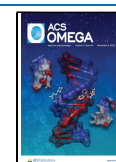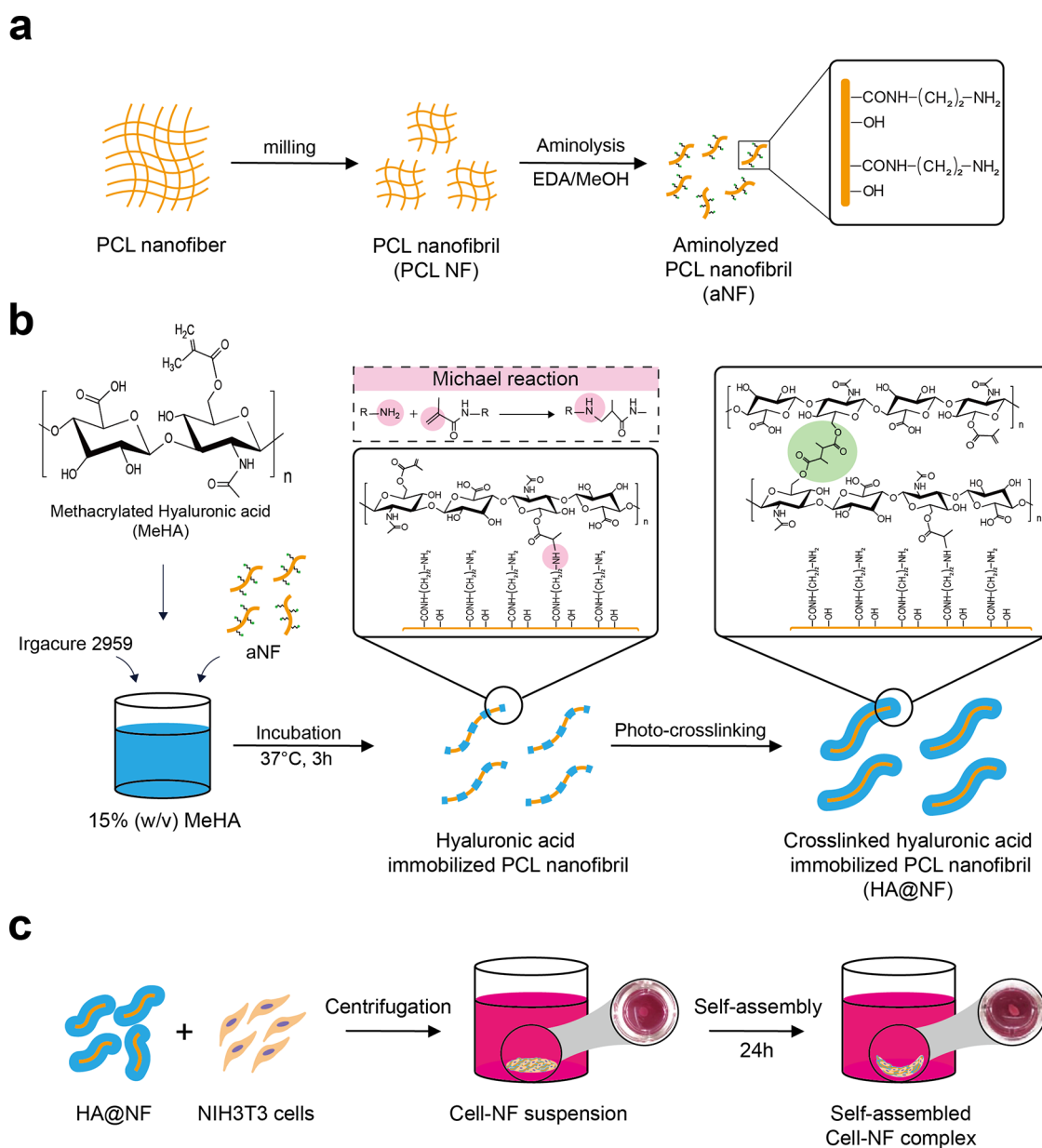
Figure 1. Schematic representation of HA immobilized PCL nanofibril fabrication and formation of cell/NF complex. (a) Fragmentation and aminolysis of PCL nanofibrils. (b) Immobilization and photo-cross-linking of hyaluronic acid on NF for different periods (HA#@NF, # = cross-linking duration). (d) Incubation of HA@NF and NIH3T3 cells in a 96-well U-bottom plate and the observation of the spontaneously formed cell/NF complex within 24 h. Inset images represent the cell/NF suspension and complex, respectively.

surface of the nanofibers, which can participate in the chemical immobilization of bioactive molecules.[19] In our previous study, we developed a nanofibrillar PCL scaffold immobilized with gelatin methacrylate (GelMA). Fragmented PCL nanofibers were hydrolyzed and subsequently aminolyzed before the immobilization of GelMA on their surface. Aminolysis could promote a significant increase in the number of amine groups grafted on the fragmented PCL nanofiber compared to nanofibers made of a PCL-PEI block copolymer. A high amount of amine groups not only changed the surface charge but also contributed to the increased incorporation of GelMA on the surface of the PCL nanofibers.[20]

In this study, we surface-decorated aminolyzed nanofibers (aNFs) with HA via Michael-type addition and by photo-cross-linking. After spectroscopic confirmation of surface immobilization of HA, surface-wettability, thermogravimetric, and

physicochemical analyses of nanofibers were performed to determine the degree of HA immobilization on the surface of aNF. After using HA immobilized nanofibril as a cell culture matrix, we analyzed the effects of HA immobilization on cell/matrix complex formation and cell viability. Immobilization of HA on aNFs significantly enhanced the viability and proliferation of NIH3T3 cells by the formation of a cell/matrix complex, and the viability and proliferation increased with increasing degree of HA immobilization.

◼ RESULTS AND DISCUSSION

The synthesis of NFs via electrospinning and subsequent surface decoration of HA by photo-cross-linking is shown in Figure 1. To prepare aNFs, electrospun PCL nanofibers were physically fragmented and aminolyzed using optimized conditions (Figure 1a),[20] and the amount of primary amine
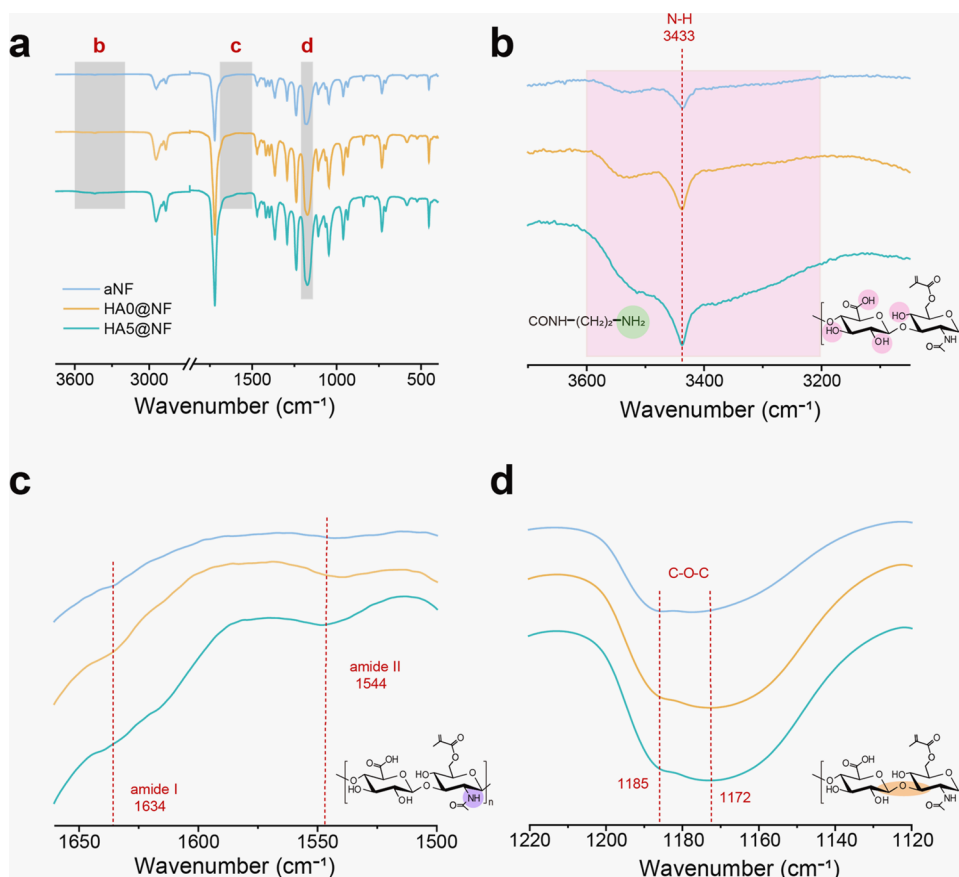
Figure 2. Fourier transform infrared (FTIR) spectra of aNF and HA#@NFs (# = 0 and 5) in the ranges of (a) 4000−400 cm^{-1}, (b) 3700−3150 cm^{-1}, (c) 1700−1500 cm^{-1}, and (d) 1220−1120 cm^{-1}.

groups on the aNFs was calculated to be 32.8 ± 6.51 nmol/mg using fluorescamine assay. After MeHA synthesis, we confirmed methacrylation by ^{1}H-NMR, where the methacryloyl group in MeHA exhibited two distinct peaks of the vinyl groups (5.6 and 6.2 ppm) (Figure S1). The degree of substitution was 11.5% based on the peak area of the methacryloyl proton in MeHA.[21] MeHA was subsequently surface-decorated on aNFs via Michael type addtion and by photo-cross-linking.[22] We hypothesize that the Michael-type addition between the primary amine group of aNFs and the methacryloyl group of MeHA is responsible for the immobilization of HA in a monolayer on the aNFs, and an additional HA layer could be formed by photo-cross-linking among the HA chains by a photoinitiator (Figure 1b,c). Spontaneous assembly of cell/NF complexes was observed when NFs with varying degrees of HA decoration and cells were cultivated in nontreated cell culture dishes (Figure S3).[23,24]

The HA immobilization of aNFs was characterized via FTIR spectroscopy (Figure 2). Broad bands for the hydroxyl groups of HA (3600−3200 cm^{-1}) were observed in HA5@NF in comparison to aNF or HA0@NF, which only exhibited a distinct band for N−H (~3433 cm^{-1}) (Figure 2b). Furthermore, HA immobilization onto NFs is considered to occur via a Michael-type addition.[25] The bands of the NFs at 1634 and 1544 cm^{-1} can be assigned to amide I and amide II attributed to the carbonyl stretching and N−H bending of HA, respectively.[26] They became more evident in HA5@NF in comparison to aNF and HA0@NF (Figure 2c). A distinct C−

O−C vibration band (1185−1172 cm^{-1}) corresponding to the glycosidic bond of HA was observed, indicating the surface immobilization of HA.[27] The C−O−C band was observed for HA5@NF, whereas the band was either absent or less intense in aNF and HA0@NF (Figure 2d). These results indicate that HA can be chemically cross-linked by photo-irradiation proportional to the irradiation duration. Thus, we hypothesize that the successful decoration of MeHA on the aNFs was due to the chemical interaction between MeHA and aNFs by Michael-type addition and photo-cross-linking.

The surface morphologies of HA@NFs and native aNFs were similar; all fragmented fibrils exhibited rough surfaces with an average length of 8.45 μm and a relatively wide (2−16 μm) size distribution. Similarly, diameters ranged from 1.6 to 3.6 μm with an average diameter of 2.19 μm. (Figure 3a). Our previous study indicated that the surface of aNFs was rougher than that of native PCL NFs.[20] This could be ascribed to the partial hydrolysis of the ester bonds in PCL, which eventually resulted in the partial erosion of the surfaces. Therefore, we hypothesized that the rough surface on the aNFs can maximize the surface area and increase HA decoration.[28] The relative amount of MeHA on individual HA@NFs was quantified by TGA (Figure 3b). MeHA exhibits a two-stage thermal decomposition curve involving a water loss curve from 60 to 100 °C, which could be attributed to the evaporation of water that bonds to the HA, and a distinctive decomposition curve from 200 to 300 °C, which resulted from the thermal breakdown of MeHA.[29] In addition, although MeHA was heated up to 698 °C, there still remained MeHA residual
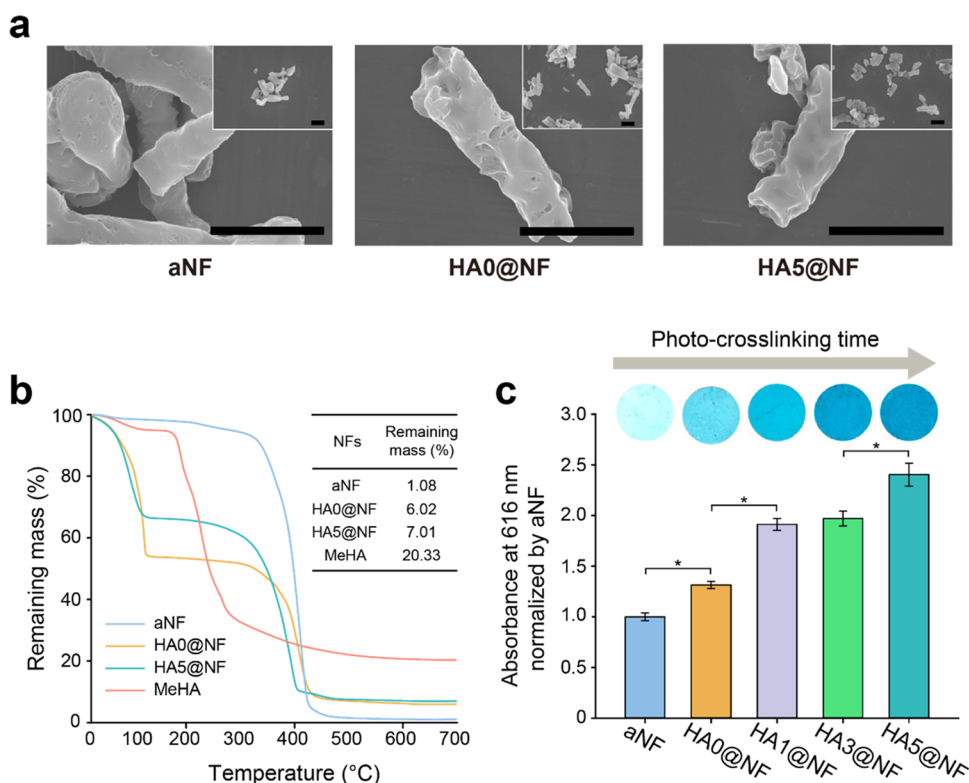
Figure 3. Physicochemical characterization of HA@NFs. (a) Morphology of nanofibrils before and after MeHA immobilization examined by field-emission scanning electron microscopy (FE-SEM). Scale bar = 5 μm. (b) Thermogravimetric analysis (TGA) curves of nanofibrils. The inset table in (b) represents the remaining mass (%) of each nanofibril at 698 °C. (c) Colorimetric analysis at 616 nm after staining by Alcian blue. The inset images in (c) represent HA@NFs with increased photo-cross-linking time, stained with Alcian blue. HA#@NFs are NFs with different HA contents, where # indicates the photo-irradiation duration. Asterisks indicate statistical significance ($p < 0.05$) evaluated by one-way ANOVA.
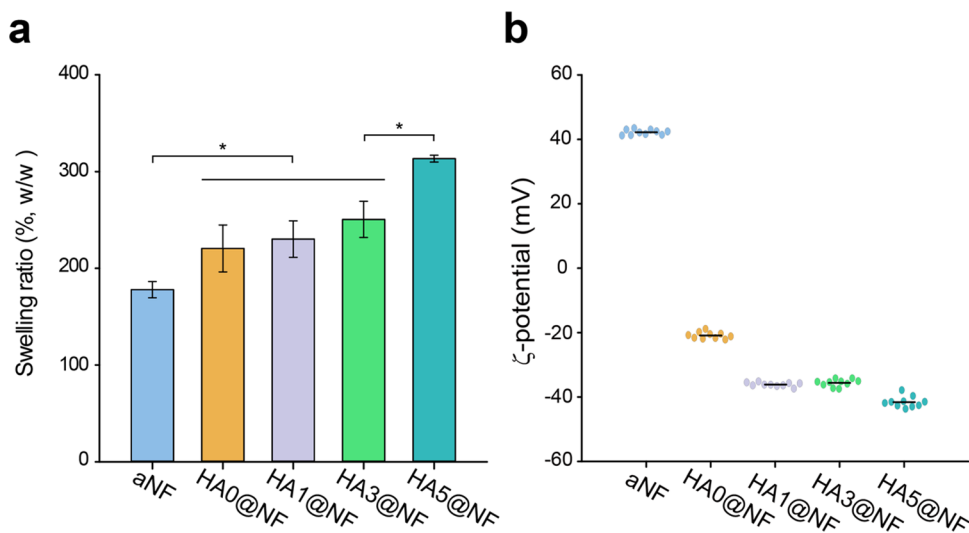

Figure 4. Physicochemical changes after MeHA immobilization. (a) Swelling ratio of HA@NFs evaluated after 3 h of incubation in DW at 37 °C. (b) ζ-potential of HA@NFs dispersed in distilled water determined by dynamic light scattering. Asterisks indicate statistical significance evaluated by one-way ANOVA ($p < 0.05$).

(20.33%). In contrast, aNF showed a consecutive decomposition curve from 300 to 400 °C, in which range the aminolyzed PCL was almost completely thermolyzed with only little residual (1.08%). These results were consistent with previous studies that showed that natural polymer HA exhibits remaining residuals even after pyrolysis at 700 °C, whereas synthetic polymer PCL could be completely decomposed.[30] HA@NF was composed of MeHA and aminolyzed PCL; therefore, HA@NF exhibited a three-stage thermal decomposition curve combining the MeHA curve and the aNF curve. Moreover, HA5@NFs (7.01%) showed higher remaining mass than HA0@NFs (6.02%), indicating that HA5@NF was immobilized with a higher amount of MeHA. Since NFs without HA were thermally degraded, we hypothesize that the relative amount of HA on HA5@NF is 1.21 times higher than that of HA0@NF. It is anticipated that HA could be
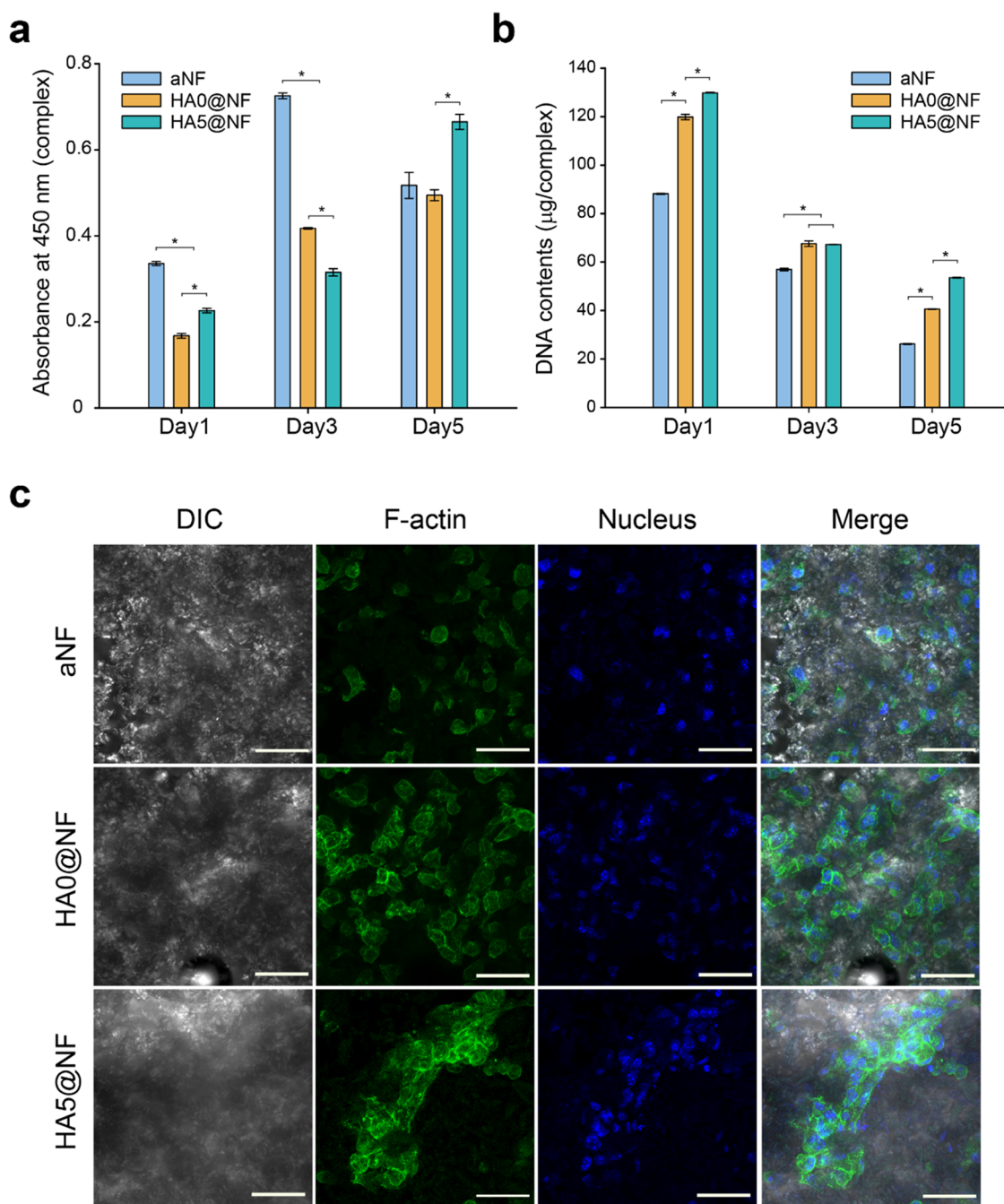
Figure 5. Proliferation rate of NIH3T3 cells and DNA contents of cell/NF complexes cultured for 1, 3, and 5 days. (a) Proliferation rate of NIH3T3 cells in the cell/NF complex estimated by WST-1-based cell viability assay. (b) DNA of each cell/NF complex quantified by picogreen DNA assay. (c) Confocal laser scanning microscopic images of cells self-assembled with aNF, HA0@NF, and HA5@NF cultivated for 72 h. F-actin and the nuclei of cell/NF complexes were stained with Alexa Fluor 488 Phalloidin and 4′,6-diamidino-2-phenylindole (DAPI), respectively. Scale bar = 50 μm. Asterisks indicate statistical significance evaluated by one-way ANOVA ($p < 0.05$).

conjugated on the aNF surfaces via a Michael-type addition, and photo-cross-linking could further increase the degree of HA decoration by immobilizing HA to aNFs. However, no significant differences were observed in the TGA thermograms of the photo-irradiated HA@NFs because of the low sensitivity of TGA (data not shown).

Surface decoration of HA was visualized by Alcian blue staining, and a gradual increase in the intensity of the blue color was observed proportional to the photo-irradiation duration (0−5 min, Figure 3c). Alcian blue specifically binds to acidic polysaccharides;[31] therefore, these results indicate that

the degree of HA immobilization to NFs is proportional to the photo-irradiation time. In comparison to NF with HA-immobilized only via Michael-type addition (HA0@NF), the staining intensities of HA1@NF, HA3@NF, and HA5@NF were 1.45, 1.50, and 1.83 times higher, respectively. Although NMR analysis is one of the methods to confirm hyaluronic acid immobilization on aNFs, however, because of poor solubility of HA@NFs both in the aqueous and organic phase, we alternatively conducted colorimetric assay to confirm the HA immobilization difference among HA#@NFs. It was confirmed that chemical immobilization is an effective method for

grafting HA on NFs, and the degree of HA immobilization could be changed by varying the photo-irradiation duration.

To investigate the swelling behavior of HA@NFs, we monitored the swelling ratio of HA@NFs after soaking them in distilled water for 3 h (Figure 4a). Compared to aNFs, all HA@NFs exhibited a higher swelling ratio; however, no significant difference was observed between HA-mono layered NFs (HA0@NF) and HA-cross-linked NFs using a short photo-irradiation duration (HA1@NF, HA3@NF). The swelling ratio for HA5@NF was higher compared to other NFs, which indicates that 5 min is the threshold photo-irradiation time to immobilize an adequate amount of MeHA onto the NFs to confer noticeable wettability, and this threshold time changing the property of HA@NFs corresponds to initial gelation time of MeHA (15% (w/v)) (Figure S2). Therefore, we expect that after 5 min of photo-cross-linking, an MeHA hydrogel layer could be formed on the surface of HA5@NF.

The surface charge of HA@NFs was affected by the photo-irradiation duration. A moderate decrease in the surface charge was observed when the photo-irradiation duration increased from 0 to 5 min. The ζ potential of the unmodified aNF was 42.2 mV; however, the ζ potential was reduced to −20.9, −36.1, −35.6, and −41.6 mV for HA0@NF, HA1@NF, HA3@NF, and HA5@NF, respectively (Figure 4. Although the degree of immobilization of HA on NFs could be controlled by adjusting the photo-irradiation duration (Figure 3), we hypothesize that a certain threshold of surface-immobilized HA is required to improve the wettability of the surface-decorated NFs, which is expected to influence cell adhesion and viability.[32] The surface charge and wettability can affect the cell adhesion on the polymer surface. The highest affinity for fibroblast adhesion was due to the combined effect of hydrophilicity and positive charge, while the lowest affinity was due to hydrophobicity and negative charge.[33] Scaffolds containing HA facilitate the upregulation of CD44 and TGF-β1 in proportion to HA, and HA and CD44 are known to result in the proliferative response to TGF-β1 in fibroblasts in an HA-rich environment.[34,35]

To investigate the effect of hyaluronic acid on the formation of a cell/NF complex, we cultivated NIH3T3 cells with HA@NFs to produce a cell/NF complex via cell-directed assembly. Cell/NF complexes formed at 24 h post seeding, and the integrity of the complexes was affected by the HA immobilization degree on HA@NFs. HA5@NF formed a tighter and thicker complex with cells, whereas the complexes formed by cells and HA0@NF or aNF were weaker and more brittle even at 48 h post seeding (Figure S3). The metabolic activities and DNA contents of cells in the cell/NF complexes were evaluated for 5 days (Figure 5). The WST-1-based metabolic activity results indicated that cells on aNFs exhibited higher viability than those on HA0@NFs or HA5@NFs within 3 days (Figure 5a). On day 5, however, cells complexed with HA5@NFs displayed 1.34 times and 1.28 times higher viability than those complexed with HA0@NFs and aNFs, respectively. On the other hand, cells complexed with aNF showeda significant decrease (0.72−0.51) in metabolic activity on day 5. This result could be ascribed to too vigorous cell proliferation within an insufficient area of the aNF at the very beginning. Cells on the aNF exhibited high metabolic activity in the first 3 days when they proliferated too fast and thus led to an overcrowded environment that is unfavorable for cells to grow further and survive,[36] resulting in decreased cell viability on

day 5. It should be noted the aNF could not maintain its complex shape on day 5 and broke apart (data not shown).

To evaluate the effect of hyaluronic acid on the proliferation of the cells complexed with HA@NFs, DNA contents of cells in the cell/NF complex were measured. The DNA content of a cell/NF complex was considered to be positively correlated with the total number of cells in the complex, and the changes in the DNA content of a complex were directly correlated with cell proliferation. The DNA quantification results indicated that the DNA contents of cells complexed with HA@NFs were higher than those of cells complexed with aNF at all cultivation durations, and HA5@NF exhibited significantly higher DNA contents than HA0@NF (Figure 5b). HA is not considered to be an ideal substrate for cell adhesion due to its negative charge;[37,38] however, in our study, although the ζ potential of HA0@NF and HA5@NF was −20.9 and −41.6 mV, respectively, there was no evidence that they abate cell adhesion and proliferation.[39] Instead, the presence of HA reinforced the cell/NF complex. Despite more integrated and tighter complexes formed with HA5@NF, a gradual decrease in the DNA content was observed over time, and it was the same with the complexes formed with aNF and HA0@NF. It should be noted that the cell/NF complex is intrinsically fragile regardless of integrity; therefore, a complex could be broken and the total cell number could decrease with the increase in cultivation duration. Nevertheless, metabolic activity and DNA content of cells complexed with HA5@NF were still the highest at day 5, implying that HA5@NF was able to recruit more cells, and cells on HA@NFs were more vitalized.

Other than affecting the formation of a cell/NF complex and cell proliferation, immobilization of hyaluronic acid showed an impact on cell morphology (Figure 5c). Differences in the morphology of NIH3T3 cells were observed after cultivating them with different NFs for 72 h. Cells cultivated with HA@NFs revealed a relatively more extended shape and more intense staining of actin filaments, especially for those cultivated with HA5@NF; in contrast, the cells cultivated with aNF demonstrated a more round shape and weaker staining of the actin filament. Cell−substance adhesion is closely related to the proliferation of anchorage-dependent cells such as fibroblasts,[40] and extracellular matrix (ECM) adsorption on the surface is considered to be important for overall cell adhesion.[41] Also, the amount of HA and surface hydrophobicity of the HA-immobilized matrix needs to be tuned precisely to obtain enhanced cell adhesion and proliferation.

In this study, we manipulated the photo-cross-linking time to precisely control the amount of HA that immobilized on aNFs. The increased HA immobilization improved the hydrophilicity of the PCL NF so that cell adhesion and proliferation on the HA@NF were enhanced, and the formation of a cell/NF complex was accelerated. Our results were in good agreement with previous studies, suggesting that the immobilized hyaluronic acid on a hydrophobic substrate could provide a cell favorable surface for adhesion and proliferation.[42] Despite tremendous reports of HA decoration on nanofibers, this is the first time to precisely control the amount of HA that is immobilized on PCL nanofibrils by controlling the photo-cross-linking time.

■ CONCLUSIONS

UV irradiation effectively immobilized HA on aNF in proportion to photo-irradiation periods. A higher degree of

HA immobilization resulted in a significant difference in TGA thermograms, microscopic morphology, swelling ratios, and surface charges. HA@NF induced self-assembly of fibroblasts to form a cell sheet, and the cell proliferation as well as the cell morphology were largely affected by the degree of HA immobilization.

■ MATERIAL AND METHODS

Materials. Poly(caprolactone) (PCL) (MW 43,000) was purchased from Polysciences (Warrington, PA). Methanol, ethanol, chloroform, and 1,4-dioxane were purchased from Daejung Chemicals and Materials (Siheung, Republic of Korea). Ethylenediamine (EDA) and glycidyl methacrylate (GMA) were purchased from Junsei Chemicals (Kyoto, Japan). Oligo-hyaluronic acid (HA, MW 0.5–10,1 kDa) was purchased from Hyundai Bioland (Cheong-Ju, Republic of Korea). Tetrabutylammonium bromide (TBAB) was purchased from TCI (Tokyo, Japan). Fluorescamine and 4′,6-diamidino-2-phenylindole dihydrochloride (DAPI) were purchased from Sigma-Aldrich (St. Louis, MO). Alcian blue 8GX was purchased from Alfa Aesar (Ward Hill, MA). Dulbecco′s phosphate-buffered saline, Dulbecco′s modified Eagle′s medium (DMEM), trypsin/EDTA, streptomycin/penicillin, and fetal bovine serum (FBS) were purchased from Gibco (Grand Island, NY). Alexa Fluor 488 Phalloidin was purchased from Invitrogen (Carlsbad, CA). The mouse embryonic fibroblast cell line, NIH/3T3, was obtained from the Korean Cell Line Bank (Seoul, Republic of Korea).

Electrospinning and Fabrication of Aminolyzed PCL Nanofibrils. PCL nanofibrils (NFs) were fabricated by physical fragmentation of electrospun PCL nanofibrous meshes. To prepare PCL nanofibrous meshes, a 25% (w/v) PCL solution in a chloroform/methanol (chloroform:methanol = 3:1, v/v) mixture was electrospun at a constant flow rate of 1 mL/h through a 25G-stainless needle (ground-to-needle distance = 10 cm) at 15 kV. An electrically ground aluminum foil was used to collect the nanofibrous meshes. The electrospun nanofibers were physically fragmented using an analytical mill (A11 basic, IKA-Werke GmbH & Co, Germany) to obtain NF powder, which was subsequently aminolyzed in a 1 M EDA solution in methanol for 72 h. The aminolyzed NFs (aNFs) were sieved (pore size: 100 μm) and washed three times with excess methanol and deionized water (DW). The surface-exposed primary amine groups on the aNFs were quantified using a fluorescamine assay with minor modifications. The aNFs dissolved in 1,4-dioxane (1 mg/mL) were allowed to react with fluorescamine in acetone (0.3 mg/mL) for 30 min on an orbital shaker in the dark. The primary amine groups were quantified by measuring the fluorescence intensity at $\lambda_{ex}/\lambda_{em}$ = 390/475 nm (λ_{ex} = excitation wavelength, λ_{em} = emission wavelength) using a spectrofluorophotometer (RF-5301PC, Shimadzu, Japan) and EDA as a standard.

Synthesis of Methacrylated Hyaluronic Acid. Methacrylated hyaluronic acid (MeHA) was prepared via the reaction of HA and GMA.[43] HA (1 g) in DW (5 mL) was mixed with TBAB (2.545 g) and GMA (2.244 g) (molar ratio of HA:TBAB:GMA = 1:3:6), and the reaction was allowed to proceed in the dark for 72 h. The resultant solution was precipitated twice using an excess amount of ice-cold acetone, and the MeHA obtained was vacuum-dried. The degree of methacrylation was confirmed via ^{1}H-NMR spectroscopy (JNM-ECZ400S/L1, JEOL, Japan) at the Central Laboratory of Kangwon National University (Figure S1). The gelation of

MeHA was examined over a wide range of concentrations. Different concentrations of the MeHA solution (5−20% (w/v)) were prepared by dissolving MeHA in an Irgacure 2959 solution (0.1% (w/v)). The MeHA solutions (0.5 mL each) were placed in 15 mL glass vials and irradiated using a UV hand lamp (VL-6-LC, VilberLourmat, France) for 1, 5, 10, and 20 min (365 nm, 6 W). The gelation of MeHA solutions was assessed via a vial inverting test (Figure S2). MeHA (15% (w/v)) was selected for further experiments.

Photo-Cross-Linking of HA on NFs. The cross-linking of MeHA on the surface of aNFs was performed for different photo-irradiation durations.[44] The aNFs (200 mg) were homogeneously dispersed in an MeHA solution (20 mL, 150 mg/mL) containing 0.1% Irgacure 2959 (w/v) and incubated at 37 °C for 3 h with vigorous stirring in the dark. The resultant solution (5 mL) was placed in a 15 mL glass vial and irradiated using a UV hand lamp (VL-6-LC, VilberLourmat, France) for 1−5 min (365 nm, 6 W) with continuous stirring. The unbound MeHA was removed by extensive washing with DW, and the MeHA-grafted NFs (HA@NF) were freeze-dried for further use. To modulate the degree of grafting of HA on aNFs, we prepared different HA#@NFs, where # indicates the photo-irradiation duration in minutes.

Characterization of HA@NFs. The morphologies of the aNF and HA@NFs were examined by field-emission scanning electron microscopy (FE-SEM) (S-4800, Hitachi, Japan) at the Central Laboratory of Kangwon National University. The length and the diameter of each nanofibril were measured via SEM images using ImageJ software. To visualize MeHA grafting on the aNFs, HA@NFs were stained with Alcian blue. The HA@NFs (10 mg) were dispersed in an Alcian blue solution (0.2 mL, 1% (w/v) in 3% acetic acid, pH 2.5) and subsequently incubated for 15 min. The unreacted Alcian blue was removed by washing with excess DW. After transferring the stained HA@NFs to a 96-well plate, the absorbance was measured at 616 nm with a microplate reader (Multiskan GO, Thermo Scientific, MA), and photographs were obtained. FTIR spectra of aNFs, HA0@NFs, and HA5@NFs were obtained using an FTIR spectrometer (iS50, Thermo Fisher Scientific, MA) with a built-in ATR (diamond crystal, 45°) mode and a DTGS detector at the Kangwon Radiation Convergence Research Support Center of the Korea Basic Science Institute (KBSI), Kangwon National University. To obtain FTIR spectra, 32 scans were co-added with a spectral resolution of 4 cm^{-1}. The pyrolytic behavior of HA@NFs was evaluated by a thermogravimetric analyzer (TGA) at the Central Laboratory of Kangwon National University (STA449 F3 Jupiter, NETZSCH, Germany). The HA@NFs (22 mg) were sealed in an aluminum pan and heated from 25 to 700 °C (10 °C/min) in a nitrogen atmosphere. To determine the water-swelling rate, HA@NFs (3 mg) were hydrated in DW for 3 h, and the water-swelling rate was calculated using the following formula: swelling rate (%) = $[(W_w - W_d)/W_d] \times 100\%$, where W_w is the wet weight and W_d is the dry weight of HA@NFs. To monitor the surface charge, HA@NFs (1 mg) were homogeneously suspended in DW (1 mL), and the ζ-potential was measured using a Zetasizer Nano ZS (ZEN 3600, Malvern Instrument, U.K.) (n = 10).

Spontaneous Formation of Cell/NF Complexes. A mixture of HA@NFs and cells spontaneously assembled into cell/NF complex 24 h post seeding, and the proliferation of cells in the cell/NF complex was investigated for 5 days. NIH3T3 cells cultivated in 10% (v/v) FBS and 1% (v/v)

streptomycin/penicillin supplemented DMEM (1×10^5 cells/well) were homogeneously mixed with 0.2 mg of aNFs or HA@NFs, and the mixture (0.2 mL) was seeded into a U-shaped bottom nontreated 96-well plate. The plate was centrifuged at 300g for 3 min, and the cells−NF matrix was subsequently cultured at 37 °C and a 5% CO_2 atmosphere. The cell proliferation was assessed after 1, 3, and 5 days, using the WST-1 assay, according to the manufacturer's protocol. The entire medium was replaced with fresh DMEM (0.2 mL), after which the WST-1 reagent (20 μL, 5 mg/mL) was added, and the mixture was incubated at 37 °C for 1 h. The absorbance of the medium was measured at 450 nm using a microplate reader. To monitor the formation of cell/NF complexes and cell distribution, the complexes were fixed using a 3.7% formaldehyde solution for 30 min and stained with Alexa Fluor 488 Phalloidin and DAPI for F-actin and nuclear visualization, respectively. The stained complexes were visualized using a high-resolution confocal laser scanning microscope (LSM880, Carl Zeiss, Germany) at the Central Laboratory of Kangwon National University. The following operating conditions were used: λ_{ex}: 488 nm for Alexa Fluor 488 Phalloidin, 405 nm for DAPI, and λ_{em}: 495−634 nm for Alexa Fluor 488 Phalloidin and 410−495 nm for DAPI. To analyze the number of cells incorporated, the amount of total DNA in the cell/NF complex was measured using Quant-iT PicoGreen (Invitrogen Ltd., Paisley, U.K.) according to the manufacturer's protocol. The cell/NF complex was treated with cell lysis buffer (0.4 mL, pH 8, TE buffer supplemented with 0.1% Triton X-100 (v/v)) and mixed homogeneously. After four freeze/thaw cycles (−80 and 37 °C), the supernatant (0.05 mL) was diluted five times with TE buffer and incubated with a PicoGreen working solution (0.25 mL) for 5 min. The fluorescence intensity was measured at $\lambda_{ex}/\lambda_{em}$ = 480:520 nm using a spectrofluorophotometer (Shimadzu Corporation, Japan).

Statistical Analysis. Unless otherwise specified, all experiments were performed in triplicate, and the data are expressed as the mean ± standard deviation. Statistical analysis was performed using a one-way analysis of variance with SigmaPlot 12.0 software, and the statistical significance was set at $p < 0.05$.

ASSOCIATED CONTENT

Supporting Information

The Supporting Information is available free of charge at https://pubs.acs.org/doi/10.1021/acsomega.2c05322.

Representative ^{1}H NMR spectrum of MeHA (Figure S1), images representing gelation of various concentrations of MeHA solutions (Figure S2), and morphology of different NIH3T3/NF complexes at 48 h after seeding (Figure S3) (PDF)

AUTHOR INFORMATION

Corresponding Author

Hyuk Sang Yoo − *Department of Medical Biomaterials Engineering, Kangwon Radiation Convergence Research Support Center, and KIIT, Kangwon National University, Chuncheon 24341, Republic of Korea;* ⓘ orcid.org/0000-0002-4346-9154; Email: hsyoo@kangwon.ac.kr

Authors

Wanho Cho − *Department of Medical Biomaterials Engineering, Kangwon National University, Chuncheon 24341, Republic of Korea*

Yeonju Park − *Kangwon Radiation Convergence Research Support Center, Kangwon National University, Chuncheon 24341, Republic of Korea*

Young Mee Jung − *Kangwon Radiation Convergence Research Support Center, Department of Chemistry, and KIIT, Kangwon National University, Chuncheon 24341, Republic of Korea*

Ju Hyun Park − *Department of Medical Biomaterials Engineering and KIIT, Kangwon National University, Chuncheon 24341, Republic of Korea*

Jongmin Park − *Department of Chemistry and KIIT, Kangwon National University, Chuncheon 24341, Republic of Korea*

Complete contact information is available at:
https://pubs.acs.org/10.1021/acsomega.2c05322

Notes

The authors declare no competing financial interest.

REFERENCES

(1) Garg, K.; Bowlin, G. L. Electrospinning Jets and Nanofibrous Structures. *Biomicrofluidics* **2011**, *5*, No. 013403.

(2) Ignatova, M.; Manolova, N.; Markova, N.; Rashkov, I. Electrospun Non-Woven Nanofibrous Hybrid Mats Based on Chitosan and PLA for Wound-Dressing Applications. *Macromol. Biosci.* **2009**, *9*, 102−111.

(3) Wang, L.; Wu, Y.; Hu, T.; Guo, B.; Ma, P. X. Electrospun Conductive Nanofibrous Scaffolds for Engineering Cardiac Tissue and 3D Bioactuators. *Acta Biomater.* **2017**, *59*, 68−81.

(4) Li, D.; Xia, Y. Electrospinning of Nanofibers: Reinventing the Wheel? *Adv. Mater.* **2004**, *16*, 1151−1170.

(5) Teo, W. E.; Ramakrishna, S. A Review on Electrospinning Design and Nanofibre Assemblies. *Nanotechnology* **2006**, *17*, R89−R106.

(6) Subbiah, T.; Bhat, G. S.; Tock, R. W.; Parameswaran, S.; Ramkumar, S. S. Electrospinning of Nanofibers. *J. Appl. Polym. Sci.* **2005**, *96*, 557−569.

(7) Schiffman, J. D.; Schauer, C. L. A Review: Electrospinning of Biopolymer Nanofibers and Their Applications. *Polym. Rev.* **2008**, *48*, 317−352.

(8) Geng, X.; Kwon, O. H.; Jang, J. Electrospinning of Chitosan Dissolved in Concentrated Acetic Acid Solution. *Biomaterials* **2005**, *26*, 5427−5432.

(9) Um, I. C.; Fang, D.; Hsiao, B. S.; Okamoto, A.; Chu, B. Electro-Spinning and Electro-Blowing of Hyaluronic Acid. *Biomacromolecules* **2004**, *5*, 1428−1436.

(10) Brenner, E. K.; Schiffman, J. D.; Thompson, E. A.; Toth, L. J.; Schauer, C. L. Electrospinning of Hyaluronic Acid Nanofibers from Aqueous Ammonium Solutions. *Carbohydr. Polym.* **2012**, *87*, 926−929.

(11) Sun, K.; Li, Z. H. Preparations, Properties and Applications of Chitosan Based Nanofibers Fabricated by Electrospinning. *Express Polym. Lett.* **2011**, *5*, 342−361.

(12) Zhang, Y.; Ouyang, H.; Chwee, T. L.; Ramakrishna, S.; Huang, Z. M. Electrospinning of Gelatin Fibers and Gelatin/PCL Composite Fibrous Scaffolds. *J. Biomed. Mater. Res.* **2005**, *72B*, 156−165.

(13) Charernsriwilaiwat, N.; Rojanarata, T.; Ngawhirunpat, T.; Opanasopit, P. Electrospun Chitosan/Polyvinyl Alcohol Nanofibre Mats for Wound Healing. *Int. Wound J.* **2014**, *11*, 215−222.

(14) de Castro, K. C. d.; Burga-Sanchez, J.; Campos, M. G. N.; Mei, L. H. I. Water-Based Synthesis of Photocrosslinked Hyaluronic Acid/Polyvinyl Alcohol Membranes: Via Electrospinning. *RSC Adv.* **2020**, *10*, 31271−31279.

(15) Chen, G.; Guo, J.; Nie, J.; Ma, G. Preparation, Characterization, and Application of PEO/HA Core Shell Nanofibers Based on Electric Field Induced Phase Separation during Electrospinning. *Polymer* **2016**, *83*, 12−19.

(16) Koosha, M.; Mirzadeh, H. Electrospinning, Mechanical Properties, and Cell Behavior Study of Chitosan/PVA Nanofibers. *J. Biomed. Mater. Res., Part A* **2015**, *103*, 3081−3093.

(17) Ji, Y.; Ghosh, K.; Shu, X. Z.; Li, B.; Sokolov, J. C.; Prestwich, G. D.; Clark, R. A. F.; Rafailovich, M. H. Electrospun Three-Dimensional Hyaluronic Acid Nanofibrous Scaffolds. *Biomaterials* **2006**, *27*, 3782−3792.

(18) Mao, W.; Kang, M. K.; Shin, J. U.; Son, Y. J.; Kim, H. S.; Yoo, H. S. Coaxial Hydro-Nanofibrils for Self-Assembly of Cell Sheets Producing Skin Bilayers. *ACS Appl. Mater. Interfaces* **2018**, *10*, 43503−43511.

(19) Zhu, Y.; Gao, C.; Liu, X.; Shen, J. Surface Modification of Polycaprolactone Membrane via Aminolysis and Biomacromolecule Immobilization for Promoting Cytocompatibility of Human Endothelial Cells. *Biomacromolecules* **2002**, *3*, 1312−1319.

(20) Lee, J. W.; Yoo, H. S. Michael-Type Addition of Gelatin on Electrospun Nanofibrils for Self-Assembly of Cell Sheets Composed of Human Dermal Fibroblasts. *ACS Omega* **2019**, *4*, 18677−18684.

(21) Bencherif, S. A.; Srinivasan, A.; Horkay, F.; Hollinger, J. O.; Matyjaszewski, K.; Washburn, N. R. Influence of the Degree of Methacrylation on Hyaluronic Acid Hydrogels Properties. *Biomaterials* **2008**, *29*, 1739−1749.

(22) Jin, R.; Teixeira, L. S. M.; Krouwels, A.; Dijkstra, P. J.; Van Blitterswijk, C. A.; Karperien, M.; Feijen, J. Synthesis and Characterization of Hyaluronic Acid-Poly(Ethylene Glycol) Hydrogels via Michael Addition: An Injectable Biomaterial for Cartilage Repair. *Acta Biomater.* **2010**, *6*, 1968−1977.

(23) Kim, H. S.; Mandakhbayar, N.; Kim, H. W.; Leong, K. W.; Yoo, H. S. Protein-Reactive Nanofibrils Decorated with Cartilage-Derived Decellularized Extracellular Matrix for Osteochondral Defects. *Biomaterials* **2021**, *269*, No. 120214.

(24) Pham-Nguyen, O. V.; Shin, J. U.; Kim, H.; Yoo, H. S. Self-Assembled Cell Sheets Composed of Mesenchymal Stem Cells and Gelatin Nanofibers for the Treatment of Full-Thickness Wounds. *Biomater. Sci.* **2020**, *8*, 4535−4544.

(25) González, G.; Fernández-Francos, X.; Serra, À.; Sangermano, M.; Ramis, X. Environmentally-Friendly Processing of Thermosets by Two-Stage Sequential Aza-Michael Addition and Free-Radical Polymerization of Amine-Acrylate Mixtures. *Polym. Chem.* **2015**, *6*, 6987−6997.

(26) Carneiro, J.; Döll-Boscardin, P. M.; Fiorin, B. C.; Nadal, J. M.; Farago, P. V.; De Paula, J. P. Development and Characterization of Hyaluronic Acid-Lysine Nanoparticles with Potential as Innovative Dermal Filling. *Braz. J. Pharm. Sci.* **2016**, *52*, 645−651.

(27) Mirzayeva, T.; Čopíková, J.; Kvasnička, F.; Bleha, R.; Synytsya, A. Screening of the Chemical Composition and Identification of Hyaluronic Acid in Food Supplements by Fractionation and Fourier-Transform Infrared Spectroscopy. *Polymers* **2021**, *13*, No. 4002.

(28) Yamanlar, S.; Sant, S.; Boudou, T.; Picart, C.; Khademhosseini, A. Surface Functionalization of Hyaluronic Acid Hydrogels by Polyelectrolyte Multilayer Films. *Biomaterials* **2011**, *32*, 5590−5599.

(29) Chen, S. H.; Chen, C. H.; Shalumon, K. T.; Chen, J. P. Preparation and Characterization of Antiadhesion Barrier Film from Hyaluronic Acid-Grafted Electrospun Poly(Caprolactone) Nanofibrous Membranes for Prevention of Flexor Tendon Postoperative Peritendinous Adhesion. *Int. J. Nanomed.* **2014**, *9*, 4079−4092.

(30) Chen, C. H.; Li, D. L.; Chuang, A. D. C.; Dash, B. S.; Chen, J. P. Tension Stimulation of Tenocytes in Aligned Hyaluronic Acid/Platelet-Rich Plasma-Polycaprolactone Core-Sheath Nanofiber Membrane Scaffold for Tendon Tissue Engineering. *Int. J. Mol. Sci.* **2021**, *22*, No. 11215.

(31) Parker, B. C.; Diboll, A. G. Alcian Stains for Histochemical Localization of Acid and Sulfated Polysaccharides in Algae. *Phycologia* **1966**, *6*, 37−46.

(32) Madaboosi, N.; Uhlig, K.; Schmidt, S.; Vikulina, A. S.; Möhwald, H.; Duschl, C.; Volodkin, D. A "Cell-Friendly" Window for the Interaction of Cells with Hyaluronic Acid/Poly-l-Lysine Multilayers. *Macromol. Biosci.* **2018**, *18*, No. 1700319.

(33) Guo, S.; Zhu, X.; Li, M.; Shi, L.; Ong, J. L. T.; Jańczewski, D.; Neoh, K. G. Parallel Control over Surface Charge and Wettability Using Polyelectrolyte Architecture: Effect on Protein Adsorption and Cell Adhesion. *ACS Appl. Mater. Interfaces* **2016**, *8*, 30552−30563.

(34) Qian, Y.; Li, L.; Jiang, C.; Xu, W.; Lv, Y.; Zhong, L.; Cai, K.; Yang, L. The Effect of Hyaluronan on the Motility of Skin Dermal Fibroblasts in Nanofibrous Scaffolds. *Int. J. Biol. Macromol.* **2015**, *79*, 133−143.

(35) Meran, S.; Luo, D. D.; Simpson, R.; Martin, J.; Wells, A.; Steadman, R.; Phillips, A. O. Hyaluronan Facilitates Transforming Growth Factor-B1-Dependent Proliferation via CD44 and Epidermal Growth Factor Receptor Interaction. *J. Biol. Chem.* **2011**, *286*, 17618−17630.

(36) Carlo, D. Di; Wu, L. Y.; Lee, L. P. Dynamic Single Cell Culture Array. *Lab Chip* **2006**, *6*, 1445−1449.

(37) Lai, J. Y.; Tu, I. H. Adhesion, Phenotypic Expression, and Biosynthetic Capacity of Corneal Keratocytes on Surfaces Coated with Hyaluronic Acid of Different Molecular Weights. *Acta Biomater.* **2012**, *8*, 1068−1079.

(38) Kim, S.; Jang, Y.; Jang, M.; Lim, A.; Hardy, J. G.; Park, H. S.; Lee, J. Y. Versatile Biomimetic Conductive Polypyrrole Films Doped with Hyaluronic Acid of Different Molecular Weights. *Acta Biomater.* **2018**, *80*, 258−268.

(39) Chang, H. Y.; Huang, C. C.; Lin, K. Y.; Kao, W. L.; Liao, H. Y.; You, Y. W.; Lin, J. H.; Kuo, Y. T.; Kuo, D. Y.; Shyue, J. J. Effect of Surface Potential on NIH3T3 Cell Adhesion and Proliferation. *J. Phys. Chem. C* **2014**, *118*, 14464−14470.

(40) Vivas, J.; Garzón-Alvarado, D.; Cerrolaza, M. Modeling Cell Adhesion and Proliferation: A Cellular-Automata Based Approach. *Adv. Model. Simul. Eng. Sci.* **2015**, *2*, No. 32.

(41) Cooke, M. J.; Phillips, S. R.; Shah, D. S. H.; Athey, D.; Lakey, J. H.; Przyborski, S. A. Enhanced Cell Attachment Using a Novel Cell Culture Surface Presenting Functional Domains from Extracellular Matrix Proteins. *Cytotechnology* **2008**, *56*, 71−79.

(42) Zamboni, F.; Keays, M.; Hayes, S.; Albadarin, A. B.; Walker, G. M.; Kiely, P. A.; Collins, M. N. Enhanced Cell Viability in Hyaluronic Acid Coated Poly(Lactic-Co-Glycolic Acid) Porous Scaffolds within Microfluidic Channels. *Int. J. Pharm.* **2017**, *532*, 595−602.

(43) Baier Leach, J.; Bivens, K. A.; Patrick, C. W.; Schmidt, C. E. Photocrosslinked Hyaluronic Acid Hydrogels: Natural, Biodegradable Tissue Engineering Scaffolds. *Biotechnol. Bioeng.* **2003**, *82*, 578−589.

(44) Li, X.; Luan, S.; Shi, H.; Yang, H.; Song, L.; Jin, J.; Yin, J.; Stagnaro, P. Improved Biocompatibility of Poly (Styrene-b-(Ethylene-Co-Butylene)-b-Styrene) Elastomer by a Surface Graft Polymerization of Hyaluronic Acid. *Colloids Surf., B* **2013**, *102*, 210−217.